

USING BISPECTRAL FULL-WAVEFORM LIDAR TO MAP SEAMLESS COASTAL HABITATS IN 3D

M. Letard^{1*}, A. Collin¹, D. Lague², T. Corpetti³, Y. Pastol⁴, A. Ekelund⁵

¹ Ecole Pratique des Hautes Etudes - PSL Université, Coastal GeoEcological Lab, Dinard, France - (mathilde.letard@ephe.psl.eu)

² Univ Rennes, CNRS, Géosciences Rennes - UMR 6118 - Rennes, France - dimitri.lague@univ-rennes1.fr

³ Université Rennes 2, CNRS UMR 6554 LETG - Rennes, France - thomas.corpetti@univ-rennes2.fr

⁴ Service Hydrographique et Océanographique de la Marine - Brest, France - yves.pastol@shom.fr

⁵ Airborne Hydrography AB - Jönköping, Sweden - anders.ekelund@hexagon.com

KEY WORDS: Topobathymetric lidar, Full-waveform lidar, Classification, Coastal habitats, Habitat mapping.

ABSTRACT:

Mapping coastal habitats is essential to their preservation, but the presence of water hinders seamless data collection over land-water interfaces. Thanks to its dual-wavelength and optical properties, topo-bathymetric lidar can address this task efficiently. Topo-bathymetric lidar waveforms contain relevant information to classify land and water covers automatically but are rarely analysed for both infrared and green wavelengths. The present study introduces a point-based approach for the classification of coastal habitats using bispectral waveforms of topo-bathymetric lidar surveys and machine learning. Spectral features and differential elevations are fed to a random forest algorithm to produce three-dimensional classified point clouds of 17 land and sea covers. The resulting map reaches an overall accuracy of 86%, and 65% of the prediction probabilities are above 0.60. Using this prediction confidence, it is possible to map coastal habitats and eliminate the classification errors due to noise in the data, that generate a clear tendency of the algorithm to over-estimate some classes at the expense of some others. By filtering out points with a low prediction confidence (under 0.7), the classification can be highly improved and reach an overall accuracy of 97%.

1. INTRODUCTION

The global coastal population has been growing fast for a few decades. In 2003, 41% of the world's global population lived within 100 km of the coastline (UNPD, 2005), and 21 of the 33 world's megacities were located on coastal fringes. Moreover, Martínez et al. (2007) showed that the wide diversity of ecosystems located at the interface between the Earth's oceans and continents produced 77% of the estimated economic value of the services and goods provided by ecosystems around the world in 2007, based on the method in (Costanza et al., 1997). All of these observations converge to show how ecologically, socially and economically important coastal ecosystems are (Martínez et al., 2007, Costanza et al., 1997 and Barbier et al., 2011). However, marine and terrestrial habitats are threatened by climate change and anthropic pressure (Barbier et al., 2011), and numerous studies agree that their evolution is difficult to anticipate and must be monitored to ensure continual support to littoral communities (Barbier et al., 2001, Martínez et al., 2007, Costanza et al., 1997).

Currently, the observation of coastal ecosystems without interruption between marine and terrestrial domains remains a methodological challenge due to the presence of water, which complicates their exploration with passive imagery (Kutser et al., 2020), and due to their vast diversity. Topo-bathymetric lidar is particularly suited to the task, as an active sensor able to penetrate the water surface and collect information both on ground and on the sea- or river-bed (Philpot, 2019, Lague and Feldmann, 2020). Lidar surveys of coastal areas are mostly used as 2D rasters (Wedding et al., 2008), or 3D point clouds (Hansen et al., 2021, Tulldahl and Wikström, 2012), that are classified to study given land or sea covers. Nonetheless, the origin of lidar data, which lies in signal processing of the lidar waveforms - the complete laser signal backscattered by the

environment - and its potential contribution to coastal habitats monitoring remain underexplored. Lidar waveform analysis has been developed for topographic lidar data classification (Mallet and Bretar, 2009, Mallet et al., 2011, Reitberger et al., 2009, Zorzi et al., 2019), but little methodological research on the exploitation of bathymetric or topo-bathymetric waveforms exists. Yet, these data include more detailed information on the physical properties of the environment surveyed than the elevation contained in rasters or point clouds, by registering also the way the Earth's covers interact with light. This information is particularly useful to classify covers that have distinct spectral signatures (e.g., Letard et al., 2022) or subtle geometric features at decimeter scale that discrete echoes cannot capture (e.g. Launeau et al., 2018).

Exploiting lidar data requires adapted processing methods, as this sensor produces rich but complex information on the environment, with sometimes dozens of point records and several waveforms of up to a thousand of samples per square metre. Although efficient tools exist to process lidar derived rasters or point clouds, methods to efficiently exploit the knowledge enclosed by the waveforms are still expected, as they remain mainly experimental.

In this study, we propose a topo-bathymetric lidar waveform-based coastal habitat classification and explore its abilities to map 17 different types of marine and terrestrial covers. This method relies on the use of a random forest algorithm to classify features extracted from green and infrared (IR) lidar waveforms. The article focuses on addressing three main questions: (1) are topo-bathymetric lidar waveforms usable for detailed coastal habitat mapping?, (2) what is the added value of bispectral lidar data compared to a simple bathymetric lidar survey? and (3) what prediction confidence can we expect of our algorithm?

* Corresponding author

2. MATERIALS AND STUDY AREA

In this section, we briefly recall the operating principles of full-waveform lidar and describe our datasets.

2.1 Full-waveform lidar

Airborne lidar sensors emit laser pulses towards the ground and record the backscattered signal, from which two types of data can be obtained: lidar waveforms and lidar point clouds. Waveforms are time series of the complete backscattered signal, while point clouds are obtained through processing of the waveforms: each major peak in the waveform corresponds to an object encountered by the laser beam. The coordinates of these obstacles can be computed using the time range for the laser signal to travel back and forth, which enables the reconstitution of the whole scene surveyed into 3D point clouds. Topographic lidars operate with an IR laser, which is unable to travel through water surfaces. Topo-bathymetric lidars use a green laser in addition to the IR one, green lasers being able to reach the ground below the water surface. They are thus able to collect data on marine and terrestrial environments, without interruption between submerged or emerged domains.

Lidar waveforms contain important information on the physical properties of the objects encountered by the laser emitted, namely through the way light is reflected by them. They can therefore be used to map the Earth's covers (Collin et al., 2012, Letard et al., 2022). Each peak in the waveform has a different shape depending on what it originated from on the ground. Typical bathymetric waveforms have the particularity of integrating three main components: a peak produced by the water surface and elongated by a water column component, and another peak corresponding to the bottom if it is reached. Two typical waveform examples are presented in Figure 1.

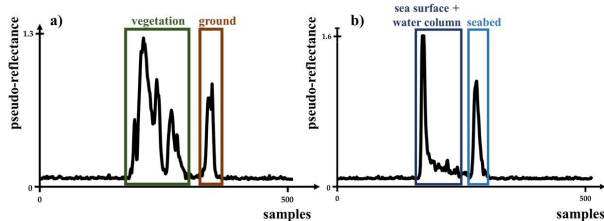


Figure 1. Typical example of a) a bathymetric waveform and b) a topographic waveform.

2.2 Lidar dataset

The lidar dataset was acquired in September 2019 for the Litto 3D[®] (Shom et al., 2021) project operated by the French Hydrographic Office (Shom). It was collected with a Leica HawkEye III full-waveform topo-bathymetric lidar using wavelengths at 1064 nm and 515 nm and collecting data with an elliptic pattern. Each green waveform and every 32 IR waveforms were recorded with a time frequency of 1.8 GHz, resulting in a backscattered intensity value every 556 picoseconds. The survey was led with a constant laser amplification, and the intensity of each emitted pulse linked to a waveform is available. There are on average 6.7 green waveforms and 0.5 IR waveforms per square metre. The green laser's spot size diameter is 1.8 m, while the IR laser's is 0.2 m.

2.3 Study area and ground-truth data acquisition

The study area is located on the coasts of Brittany, France in a town called Sables d'Or les Pins (48.6373, -2.4067). It features typical coastal habitats such as salt marshes, seagrasses, sandy

dunes, sandy beaches, pebble beaches, pine trees or macroalgae. It is presented in Figure 2.

A ground-truth data acquisition campaign took place in 2021 to gather knowledge on the land and sea covers in this area, through unmanned airborne vehicles (UAV) and unmanned surface vehicle (USV) RGB imagery. Figure 2 shows the areas covered by these acquisitions. The UAV used was a RGB DJI Phantom 4 Pro V2, and the USV was a PowerVision PowerDolphin. The UAV flights were calibrated with a total of 55 ground control points. 150 geolocated photoquadrats were also collected on site. Photogrammetric reconstructions of the UAV images, and an RGB orthoimage from 2014 were used to create the labelled lidar training and test datasets (necessary to perform habitat classification) via photointerpretation.

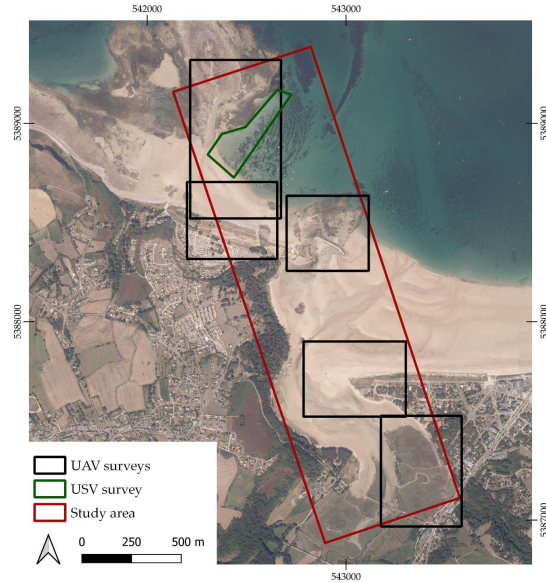


Figure 2. The area studied, and the location of the 6 ground-truth data acquisitions (WGS 84/UTM 30N).

3. METHOD

In this study, we evaluate a point-based classification method relying on the classification of features extracted from bispectral waveforms. Green and IR waveforms are first processed to extract features describing them. The attributes obtained with each wavelength are then matched in a single dataset and fed to a random forest algorithm to be classified into 16 classes. These classes are presented and illustrated in Table 1.

Class name	Illustration	Class name	Illustration
Algae		Seagrass	
Submerged sand		Submerged rock	
Rock		Pebble	


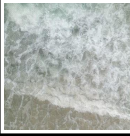



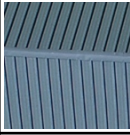





Wet sand		Surf zone	
Dry sand		Artificial ground	
Boat		Roof	
Car		Salt marsh	
Low vegetation (lawn)		Intermediate vegetation (shrub)	
Tree			

Table 1. Presentation of the land and sea covers classes studied.

3.1 Extraction of spectral features from the lidar waveforms and constitution of a bispectral dataset

To extract parameters describing the ground modelled by the waveforms, the peaks corresponding to the ground cover had to be isolated from the noise (topographic waveforms) and from the water components (bathymetric covers). All waveforms are first divided by the emitted intensity of the laser pulse they reflected. They are then smoothed using a Savitzky-Golay filter to attenuate the noise. Green and IR waveforms were not processed the same way since they do not have the same behaviour in the presence of water. In both cases, the first-derivative of the waveform was computed and thresholded in order to detect peaks in the signals and isolate the noise.

For green waveforms, if more than one peak were detected, features were computed on the group of peaks located after this first peak. The exponential decay of the lidar waveform under the influence of water was corrected as explained in (Letard et al., 2021). If only one peak was identified, features were computed on this peak.

For IR waveforms, features were computed on the group of peaks identified. The features are presented in Table 2.

Feature name	Definition
Complexity	Number of sign changes of the first derivative
Mean	Mean pseudo-reflectance
Median	Median pseudo-reflectance
Maximum	Maximum pseudo-reflectance
Standard deviation	Standard deviation of the pseudo-reflectance
Skewness	Skewness of the peak
Kurtosis	Kurtosis of the peak
Area under curve (AUC)	Area under the curve formed by the peak

Time range	Time duration of the peak
Height	Difference of elevation between the beginning and the end of the peak
Position of the maximum	Position of the maximum in the peak (in sample indices)
Difference of elevation (DZ)	Difference between the elevation of the IR return and the green return

Table 2. Definition of the features extracted in the waveforms.

These features were computed for each waveform, resulting in two sets of waveform features: a green waveform features dataset and an IR waveform features dataset. They were combined into a bispectral dataset using a nearest neighbour matching method: each green waveform features set was associated to its closest neighbour in the IR waveforms features dataset. This was made using the software “CloudCompare” (Girardeau-Montaut, 2016), which relies on the euclidean 3D distance of each point to the rest of the cloud’s components to find its nearest neighbour.

3.2 Random forest classification

The features were computed as attributes of the points forming the two point clouds, in order to avoid any information loss that could occur when rasterizing the data. These point clouds were then directly classified into the 16 classes defined above.

A random forest classifier was chosen for its performance on multiclass problems implying dozens of features and its robustness to overfitting. The possibility to retrieve feature importance and prediction probability made it particularly suited to our needs. This algorithm has also been tested multiple times in 3D point clouds classification research, with consistent observations of high accuracy in land cover identification (Yan et al., 2015, Chehata et al., 2009). The random forest model employed was set to contain 150 trees and classical parameters. We used the implementation of the “scikit-learn” library (Pedregosa et al., 2011).

A set of 1000 samples of each class was used to train the model. Another set of 500 distinct samples of each class were then used to assess the quality of the model’s predictions. These samples form the training and test datasets of 16000 and 8000 feature sets respectively, that are shown in Figure 3.

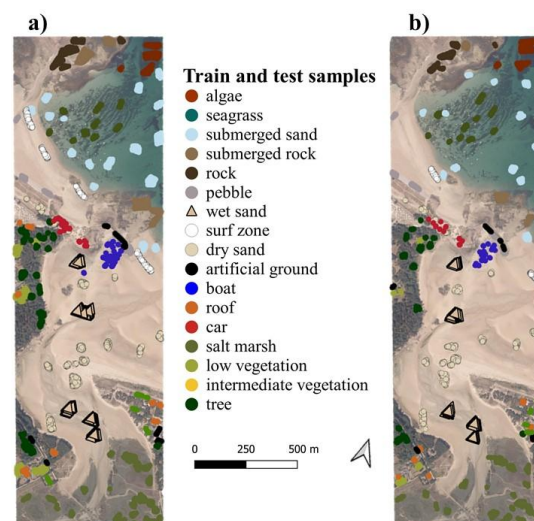


Figure 3. Distribution of the distinct a) train and b) test samples across the studied area (the natural colored imagery was acquired four years prior to the lidar survey).

3.3 Classification result assessment

To quantify the performances of our classifier, the overall accuracy (proportion of correct predictions, best when its value is 1), the average precision (proportion of correct detections of each label, best when its value is 1), the average recall (proportion of points of each label that are identified correctly, best when its value is 1) and the average F-score (combination of precision and recall, best when its value is 1) were computed for each classification on the test dataset (data that were never seen by the algorithm during training).

A class-wise analysis was also performed, by detailing the metrics obtained for each class for each experiment.

3.4 Feature selection

To avoid potential negative feedback on the classification accuracy due to information redundancy among the 24 predictors, an importance analysis was performed to select the most relevant attributes for the final habitat map. To evaluate the contribution of each predictor to the overall classification accuracy, they were each successively dropped to compare the overall accuracy obtained without them to the reference accuracy obtained on the complete set of features. The predictors that contributed negatively to the classification accuracy were removed from the classification attributes.

3.5 Production of a 3D habitat classification

The output of our method consisted in a set of labelled waveform features vectors. Using the coordinates of each waveform, this dataset was turned into a 3D point cloud of the terrestrial and marine habitats of Sables d'Or les Pins.

4. RESULTS

4.1 Results obtained with different sets of predictors

Classification experiments were led on five different sets of predictors in order to evaluate their relevance and added-value. These five sets are the following:

- all green waveform features (11 features)
- all IR waveform features (11 features)
- DZ (one feature only)
- green and IR waveform features (22 features)
- all waveform features, plus DZ (23 features)

The performances of the classifications obtained for these sets are presented in Table 3.

Model	OA	Precision	Recall	F-score
Green	0.823	0.825	0.823	0.821
IR	0.315	0.309	0.314	0.292
DZ	0.216	0.218	0.215	0.216
Green + IR	0.846	0.85	0.846	0.842
Green + IR +DZ	0.848	0.854	0.848	0.843

Table 3. Classification performances for different predictors.

Overall, the most relevant predictors for the classification of coastal land and sea covers are descriptors of the green lidar waveforms. IR data or differential elevation values appear to misclassify more than two thirds of the points.

4.2 Classification performances difference between both wavelengths

Since each wavelength of the topo-bathymetric lidar was designed to survey a specific type of environment (IR laser for topography and green laser for bathymetry), we performed an in-depth analysis of the classification results obtained using successively green data only and green + IR data. This analysis features the mean precision and recall obtained for each class. It allowed us to observe which type of habitat was best described by each wavelength. The mean prediction confidence obtained for each point is also taken into account, in order to better understand the potential classification errors and what they imply. This prediction confidence corresponds to the probability of membership of each point to the class it was assigned. The complete class-wise analysis conducted for the green model, and the Green + IR + DZ model are presented in Figure 4.

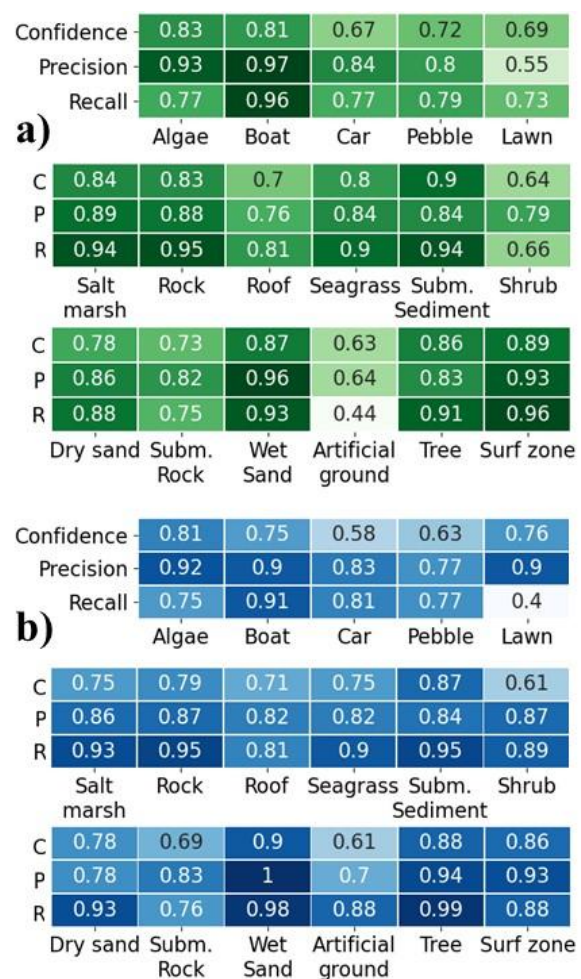


Figure 4. Class-wise classification metrics obtained when using a) green and b) bispectral waveform features as predictors.

The use of green waveform parameters produced an accurate labelling, though the algorithm showed weaker performances on topographic classes as *lawn* and *artificial ground*. The combination of both wavelengths and DZ produces a more accurate result and improves the recall of every class except low vegetation (*lawn*). Class-wise recall and precision values reveal that some classes were overestimated at the expense of others. This is the case of *submerged rock*, *algae* and *lawn*, which have lower recall values than precision.

4.3 Bispectral dataset classification

To generate the final coastal habitat classification, we analysed the contribution of each feature to the overall accuracy, and excluded from the predictors the features that impacted it negatively: green waveforms' skewness, IR waveforms' AUC, IR waveforms' skewness, IR waveforms' maximum and IR waveforms' mean. The metrics and the map obtained with the final set of features are presented in Table 5 and Figure 5.

OA	Precision	Recall	F-score
0.856	0.862	0.856	0.852

Table 5. Performance metrics obtained after selecting the features based on their contribution to the classification.

Selecting attributes based on their importance makes the overall accuracy reach 86%. Globally, the classifier's tendency to overestimate *submerged rock* or *algae* identified with the low recall in Figure 4 is observable in Figure 5, where these classes respectively invade the seagrass meadow and the surf zone.

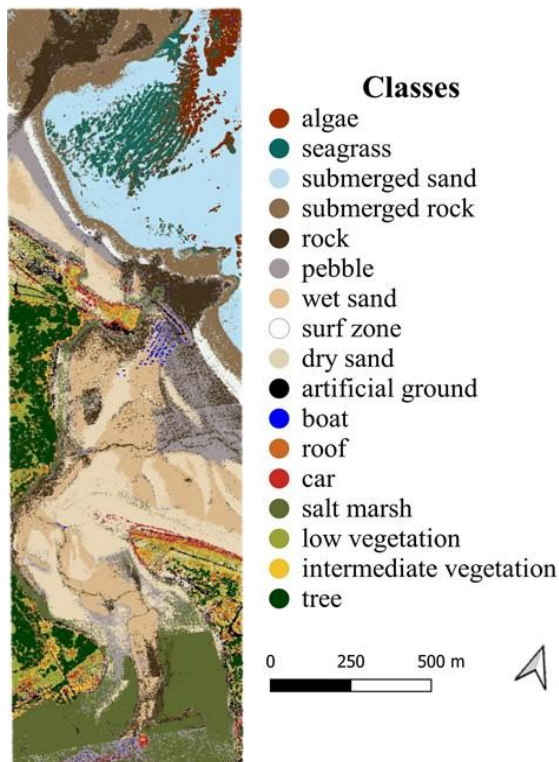


Figure 5. Coastal habitats map obtained when classifying a selected set of bispectral waveform features.

Other obvious confusions exist between *rock* and *dry sand*, or *submerged rock* and *surf zone* or *submerged sediment*. They are also revealed by the precision and recall values of these classes in Table 4. One of the main confusions is between *pebble* and sand; yet it is not as clearly quantified by the metrics.

4.4 Prediction confidence analysis

To further assess the abilities of our method to classify land and sea covers, we analysed the prediction confidence across the studied area. Figure 6 shows the maps obtained when setting a confidence threshold, below which the points are labelled as *unclassified*. Most points are kept with a threshold set at 70% (which means the probability that the point belongs to the class it was given is at least 70%). This is in line with the mean

confidence of 77% obtained on the test dataset (see Figure 4). However, when the threshold is increased at 90%, more complex areas, mainly at the interface between different classes, disappear, as they are classified with a lower confidence.

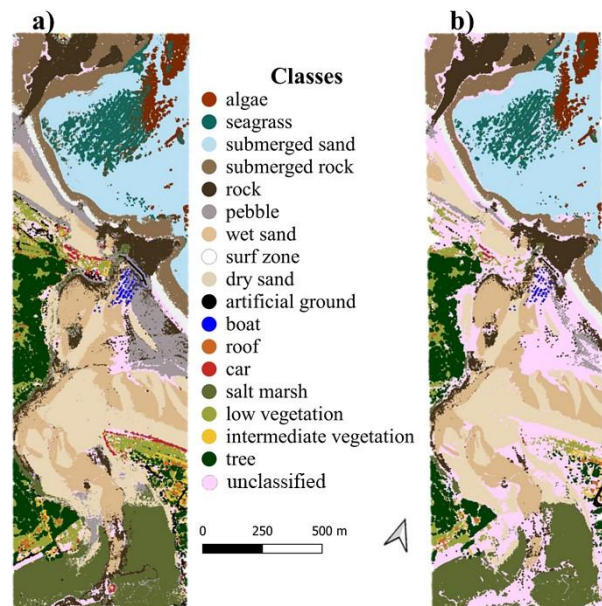


Figure 6. Land and sea covers map obtained at a) a 70% confidence level and b) a 90% confidence level.

A closer look at the misclassified samples shows that the confidence level is globally lower for them. Indeed, on the test dataset, samples that were wrongfully classified have a median confidence of 47% with a standard deviation of 17%. The overall accuracy values obtained when filtering the points based on their confidence predictions confirm that misclassified points can be discarded using this criteria: Table 6 presents the accuracies obtained for different confidence thresholds.

Threshold	0.6	0.7	0.8	0.9
OA	0.95	0.97	0.98	0.99

Table 5. Overall accuracy of the resulting classification depending on the prediction confidence threshold.

5. DISCUSSION

5.1 Usability of full-waveform lidar for coastal habitat mapping

The final result obtained confirms the observations of (Mallet et al., 2011, Letard et al., 2022, Collin et al., 2012) and the potential of lidar waveforms for classification tasks. Here, a single dataset made the classification of 17 different land and sea covers possible with high accuracy (86%, see Table 4). The resulting 3D map is presented in Figure 7. It is dense and has a high spatial resolution, suited to the realisation of ecological assessments such as ecosystem services evaluation, as performed in Martínez et al. (2007) and Costanza et al. (1997). Considering the thematic objectives of this research, the results are promising, since all habitats that provide goods and services are described with a relatively high precision (on average, 87%, see Figure 4) and in 3D, contrary to other methods developed in existing papers (Collin et al., 2012, Letard et al., 2021).

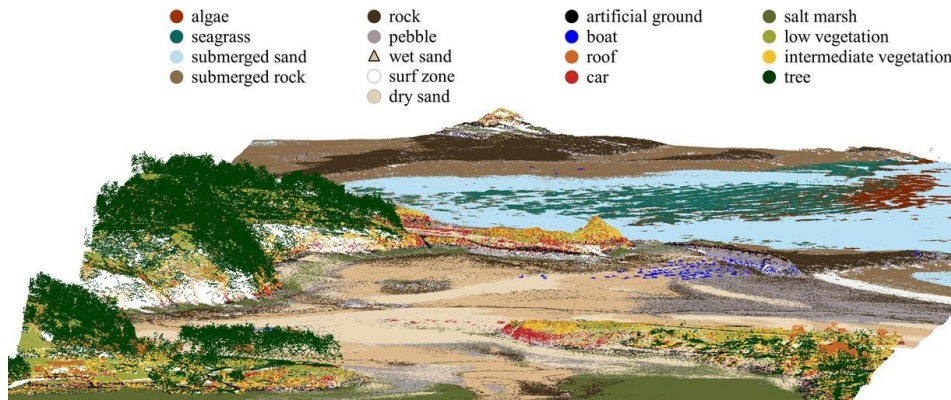


Figure 7. Resulting 3D point cloud of a coastal area and its habitats classified with full-waveform topo-bathymetric lidar

One of the main objectives of this study was to develop a method for seamless spatial modelisation of marine and terrestrial habitats. Here, the land-water continuum is classified without interruption, which is a key methodological aspect of coastal habitat monitoring (Collin et al., 2012). Figure 7 shows that the output of the classification produces an uninterrupted restitution of the land-water interface. However, our approach has limitations that necessitate further investigation: the classifier has a tendency to overestimate *algae* at the expense of *seagrass*, and *pebble* at the expense of sand, for example, as observed in previous research (Letard et al. 2022). Even though these classes are close semantically and can have similar waveform signatures due to their size, physical properties, and texture relative to the laser spot size, a better distinction is needed for ecological applications. *Boat* and *car* are also often falsely detected. Figures 5 and 7 illustrate well this issue, as a great number of points are classified as *car* on land, and part of the boulders of the dyke are labelled as *boat*. Figure 8 focuses on the sandy dune, which features many false detections of *car*.

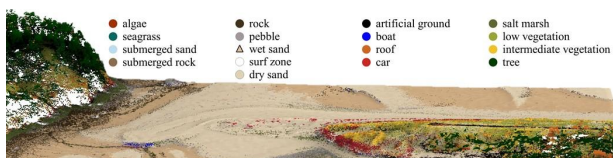


Figure 8. Extract of the resulting 3D classification: the sandy dune of Sables d’Or les Pins and its surroundings.

These errors may be explained by the albedo of cars and boats, which can vary considerably between two different types of vehicles. The wide colour spectrum they can have is difficult to model in a training dataset which can lead the classifier to learn confused information. The procedure to adopt with such classes in order not to compromise the wider objective - ecological monitoring - should be further discussed. These classes could be merged in a more global *vehicles* class, or an *unclassified* class could be added to handle unusual feature vectors and avoid their detection at the expense of natural habitats mapping, as in Figure 8 where the sandy dune - a key ecosystem - is mapped as *car*. Despite these mistakes, the possibility to have 3D assessments of the spatial repartition of different ecosystems already bears encouraging perspectives for coastal ecology, and could enhance results outlined by previous studies using rasterized topo-bathymetric lidar data (Wedding et al., 2008, Collin et al., 2012). The highly informative content of lidar waveforms, already stated in existing research on the topic (Mallet et al., 2011, Collin et al., 2012) is illustrated by their constant contribution to the resulting classification accuracy (Table 3). Lidar waveforms contain enough information to

describe surface covers, despite their lack of information on their neighbourhood’s geometry and spatial repartition (Table 3). This loss of spatial context information - compared to point cloud classification techniques involving neighbourhoods (Brodu and Lague, 2012) - is also one of the strengths of waveform-based processing. It avoids spatial averaging of information that can result in classification artefacts depending on the neighbourhood radius defined (Brodu and Lague, 2012). Classifications based on waveforms and not on spatial context may consequently gain in horizontal resolution, keeping in mind the influence of the laser’s footprint diameter (Letard et al., 2022). However, both wavelengths do not perform equally, as expected since they were each specifically designed for different environments (Philpot, 2019). Infrared waveforms cannot be used alone to study both dry and wet environments: the metrics obtained for the IR model (Table 3) quantify the limitations of topographic lidar for the survey of highly diverse environments, and corroborates previous research results (Letard et al. 2022). Green lidar waveform features perform better: their classification reaches 82% of overall accuracy, and similar values of precision and recall. Their ability to label some classes of ground is limited, which is why dual-wavelength datasets are relevant.

5.2 Contribution of the bispectral information

The combination of infrared and green datasets produces the most accurate classification overall, as in (Letard et al., 2022). The addition of the infrared features to the green parameters improves the distinction of the different types of grounds, and results in an increase of 3% of the overall accuracy, precision and recall. This can be explained by the properties of the lidar system: the infrared laser modelises a more concise and precise surface, while the larger size of the green laser may sometimes result in the mixing of different land covers into one single return, but is able to penetrate through water (Philpot, 2019). We suggest that the combination of two types of spot sizes and wavelengths optimises the information collected on a given area in terms of albedo, water content and surface rugosity, which all impact the waveform and characterise natural surfaces. Having two different lasers also provides a good understanding of the vertical complexity of the scene (Collin et al., 2012). Surfaces are sampled with varying sizes of laser beams thanks to the dual-laser system. A wider footprint hits a wider portion of surface at a time: it can mix information about several layers of covers and create intermediate points between the canopy and the ground. This phenomenon is documented in all laser scanning systems (Brodu and Lague, 2012). The smaller footprint of the infrared laser may not always penetrate through dense covers, but creates less mixed points. The combination of

both sources of data results in local differences of elevation and a greater vertical density over more complex surface covers and non planar areas. Bispectral lidar thus gives a more thorough review of the vertical structure of the environment, which can explain the improvement of the classification accuracy (+0.2%) when adding DZ to the predictors. Using DZ is also a way of including spatial context data, which is particularly contributive in point clouds classification (Brodu and Lague, 2012), to the model, without making it too dependent on the training area or involving neighbours.

Finally, the few predictors discarded after the importance analysis - green waveforms' skewness, IR waveforms' AUC, skewness, maximum and mean - show that both wavelengths contain relevant information. They also confirm the theoretically more exhaustive nature of the green waveform. Indeed, infrared waveforms seem to contain less essential details on the surveyed scene, as most of the features dropped after this step concerned the characteristics of the infrared return, whereas nearly all descriptive parameters of the green returns were useful to the random forest model.

5.3 Classification algorithm and prediction confidence

Overall, our observations corroborate existing research on the classification of lidar data using random forest algorithms (Yan et al., 2015, Hansen et al., 2021, Letard et al., 2022). As documented in (Letard et al., 2022), the model was quickly applied to a great number of features and points, and shows a good ability to exploit information and detect the 17 classes. The average prediction probability is 77%. This criteria and the qualitative results in Figures 5 and 6 outside the test dataset show that the classifier is robust to overfitting and is generalisable to a wider scene. The average prediction confidence being high, it can be used to filter the results and preserve the overall quality of the map even if it means compromising on the 3D density in some areas, as introduced by Brodu and Lague (2012). Table 5 and Figure 6 show how points can be removed by applying a confidence criteria in order to prioritise solid predictions, and thus improve the overall accuracy, as in Brodu and Lague (2012). The points affected by this filtering step give indications on the strengths and weaknesses of the random forest model. Misclassified points with high prediction probability are evidence of training errors. This is the case of the false detections of *submerged rock* along the surf zone, which Figure 9 shows more clearly. In Figure 9, the false detections of *submerged rock* are located along the *surf zone* points. The submerged rocks detected next to the rocks in the foreground are true positives. These mislabelled points have a confidence value higher than 90%, as Figure 6 b) reveals, which means that their descriptive features correspond to the usual range of statistics describing *submerged rock*. In this case, further investigation on the most distinctive feature of *submerged rock* could help identify the origin of the issue. A hypothesis could be that the similar DZ (i.e. water depth) of all the samples of *submerged rock* in the scene introduces a bias that causes the surf zone to be confused for *submerged rock*.

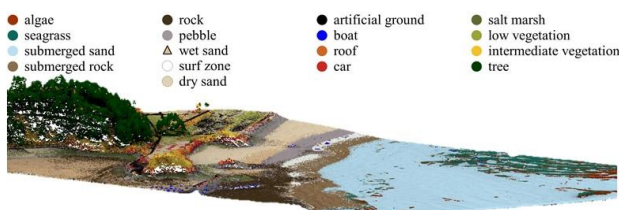


Figure 9. Extract of the resulting 3D classification: the land-water interface and its habitats.

The prediction confidence is also lower for areas at the interface between very distinct environments (Figure 6.b), where the waveforms might integrate mixed information due to the size of the laser spots. The same issue was documented in Brodu and Lague (2012) in 3D terrestrial laser scanning data classification. These areas were less documented in our training data, and the prediction probability underlines this lower confidence.

On the other hand, errors made with low confidence reveal poorly represented ranges of values among the training dataset, that are difficult to place in the possible labels. They reveal less about the training process than about the quality of the dataset. Brodu and Lague (2012) identify that some areas of 3D point clouds can have lower classification confidence due to a smaller point density compared to the rest of the scene. In their case, the classifier relies on geometrical features, and this difference in the dataset's constitution explains why their features are not as distinctive. In our case, outliers and erratic values of intensity or elevation in the data can be difficult to classify correctly, since they are not included in the training data, that are rigorously selected for their representativity of each class. In this respect, our results illustrate how important the quality of the lidar dataset is for classification tasks. Vertical or radiometric calibration issues can severely impact the possibilities to detect the nature of the surface, as we can see in Figure 5, and as suggested in Brodu and Lague (2012). Flight lines can be recognized through the classification obtained around the salt marsh and on the beach between the boat moorings and the dune. In our dataset, these lines had saturated intensities difficult to interpret, and the elevations at the interface between flight lines differed by several centimetres. The possibility to analyse the prediction confidence is thus a great indicator of the potential biases in the method. It also offers the possibility to improve the classification accuracy (Brodu and Lague, 2012): more than 10% of OA can be gained thanks to confidence-based filtering (see Table 5).

6. CONCLUSION AND OUTLOOK

In this article, we presented a method to map terrestrial and underwater habitats using a single source of data: full-waveform topobathymetric lidar. Our results show how fit this sensor is to survey diverse environments: using a random forest algorithm, we obtain classification accuracies above 85% with a mean prediction confidence of 77%. By filtering predictions depending on their classification confidence, the quality of the resulting map can be increased by up to 10%. Computing the prediction confidence also gives an interesting insight on the origin of the classification errors, which either reveal training issues, or erratic values in the initial dataset. These could be tackled with a deeper analysis of the most descriptive features for each class, and with particular attention to the calibration of the dataset and the definition of the classes during training. In the end, we obtain an interesting 3D map of 17 different land and sea covers that has potential for future ecological assessments. The presence of vertical structure information through the different spatial repartition of the points between the two wavelengths makes this result encouraging for the ecological monitoring of coastal areas. Indeed, combining vertical structure information to the knowledge waveforms provide on the physical properties of the environment could serve as ecosystem services proxy data. Lidar waveform processing also enables a finer horizontal resolution by avoiding spatial averaging of information. In future work, classifying each peak in the waveforms independently could improve the vertical density of the map to further help with ecosystem services valuation.

ACKNOWLEDGEMENTS

The authors acknowledge the financial support of the Saur Group, the Région Bretagne ARED program and the Nantes-Rennes topo-bathymetric lidar platform. They are also grateful to those who helped with data acquisitions.

REFERENCES

- Barbier, E.B., Hacker S.D., Kennedy C., Koch E.W., Stier A.C., Silliman C.R., 2011: The value of estuarine and coastal ecosystem services. *Ecological Monographs*, 81, 169-193.
- Brodu, N., Lague, D., 2012. 3D terrestrial lidar data classification of complex natural scenes using a multi-scale dimensionality criterion: Applications in geomorphology. *ISPRS Journal of Photogrammetry and Remote Sensing* 68, 121–134. <https://doi.org/10.1016/j.isprsjprs.2012.01.006>
- Chehata, N., Guo, L., Mallet, C., 2009: Airborne lidar feature selection for urban classification using random forests. In *Proceedings of the Laserscanning*, Paris, France, 1-2 September 2009.
- Collin A., Long B., Archambault P., 2012: Merging land-marine realms: spatial patterns of seamless coastal habitats using a multispectral LiDAR. *Remote Sensing of Environment*, 123, 390-399.
- Costanza, R., d'Arge, R., De Groot, R., Farber, S., Grasso, M., Hannon, B., Van Den Belt, M., 1997: The value of the world's ecosystem services and natural capital. *Nature*, 387(6630), 253-260.37.
- Girardeau-Montaut, D., 2016: CloudCompare. Available online: <https://www.danielgm.net/cc/> (accessed on 1 March 2022).
- Hansen, S.S., Ernsten, V.B., Andersen, M.S., Al-Hamdani, Z., Baran, R., Niedewieser, M., Steinbacher, F., Kroon, A., 2021: Classification of Boulders in Coastal Environments Using Random Forest Machine Learning on Topo-Bathymetric LiDAR Data. *Remote Sensing* 13, 4101, doi:10.3390/rs13204101.
- Kutser T., Vahtmäe E., Martin G., 2006: Assessing suitability of multispectral satellites for mapping benthic macroalgal cover in turbid coastal waters by means of model simulations. *Estuarine, Coastal and Shelf Science*, 67, 521-529.
- Lague, D., Feldmann, B., 2020: Chapter 2—Topo-bathymetric airborne LiDAR for fluvial-geomorphology analysis. In *Developments in Earth Surface Processes*, Tarolli, P., Mudd, S.M., Eds., Remote Sensing of Geomorphology, Elsevier: Amsterdam, The Netherlands, Volume 23, pp. 25–54.
- Launeau, P., Giraud, M., Ba, A., Moussaoui, S., Robin, M., Debaine, F., Lague, D., Le Menn, E., 2018. Full-Waveform LiDAR Pixel Analysis for Low-Growing Vegetation Mapping of Coastal Foredunes in Western France. *Remote Sensing* 10, 669. <https://doi.org/10.3390/rs10050669>
- Letard M., Collin A., Lague D., Corpetti T., Pastol Y., Ekelund A., Pergent G., Costa S., 2021: Towards 3D mapping of seagrass meadows with topo-bathymetric lidar full-waveform processing. *Proceedings of the 2021 IEEE International Geoscience and Remote Sensing Symposium IGARSS*, 8069-8072.
- Letard, M., Collin, A., Corpetti, T., Lague, D., Pastol, Y., Ekelund, A., 2022: Classification of Land-Water Continuum Habitats Using Exclusively Airborne Topobathymetric Lidar Green Waveforms and Infrared Intensity Point Clouds. *Remote Sensing* 14, 341. <https://doi.org/10.3390/rs14020341>.
- Mallet C., Bretar F., 2009: Full-waveform topographic lidar: State-of-the-art. *ISPRS Journal of Photogrammetry and Remote Sensing*, 64, 1-16.
- Mallet, C., Bretar, F., Roux, M., Soergel, U., Heipke, C., 2011. Relevance assessment of full-waveform lidar data for urban area classification. *ISPRS Journal of Photogrammetry and Remote Sensing*, Advances in LIDAR Data Processing and Applications 66, S71–S84. <https://doi.org/10.1016/j.isprsjprs.2011.09.008>.
- Martínez, M.L., Intralawan, A., Vázquez, G., Pérez-Maqueo, O., Sutton, P., Landgrave, R., 2007: The coasts of our world: Ecological, economic and social importance. *Ecological Economics*, Ecological Economics of Coastal Disasters 63, 254–272. <https://doi.org/10.1016/j.ecolecon.2006.10.022>.
- Philpot, W., 2019: *Airborne Laser Hydrography II*. doi.org/10.7298/jxm9-g971.
- Reitberger, J., Schnörr, Cl., Krzystek, P., Stilla, U., 2009: 3D segmentation of single trees exploiting full waveform LIDAR data. *ISPRS Journal of Photogrammetry and Remote Sensing* 64, 561–574. <https://doi.org/10.1016/j.isprsjprs.2009.04.002>.
- Shom, IGN, Etat Français, Région Bretagne, DREAL Bretagne, FEDER, 2021: Litto3D® Bretagne. Soon available online: <https://diffusion.shom.fr/pro/risques/altimetrie-littorale.html>.
- Tulldahl, H.M., Wikström, S.A., 2012: Classification of Aquatic Macrovegetation and Substrates with Airborne Lidar. *Remote Sens. Environ.*, 121, 347–357, doi:10.1016/j.rse.2012.02.004.
- UNDP, 2005: Human Development Report 2005: International Cooperation at a Crossroads; Aid, Trade and Security in an Unequal World. New York, USA: UNDP.
- Wedding, L.M., Friedlander, A.M., McGranaghan, M., Yost, R.S., Monaco, M.E., 2008: Using Bathymetric Lidar to Define Near-shore Benthic Habitat Complexity: Implications for Management of Reef Fish Assemblages in Hawaii. *Remote Sens. Environ.*, 112, 4159–4165, doi:10.1016/j.rse.2008.01.025.
- Yan, W.Y., Shaker, A., El-Ashmawy, N., 2015: Urban Land Cover Classification Using Airborne LiDAR Data: A Review. *Remote Sens. Environ.*, 158, 295–310, doi:10.1016/j.rse.2014.11.001.
- Zorzi, S., Maset, E., Fusiello, A., Crosilla, F., 2019: Full-Waveform Airborne LiDAR Data Classification Using Convolutional Neural Networks. *IEEE Transactions on Geoscience and Remote Sensing* 57, 8255–8261. <https://doi.org/10.1109/TGRS.2019.2919472>.